View metadata, citation and similar papers at core.ac.uk
brought to you by CORE
provided by Scientific Open-access Literature Archive and Repository

IL NUOVO CIMENTO **41 C** (2018) 109
DOI 10.1393/ncc/i2018-18109-5

COMMUNICATIONS: SIF Congress 2017

First dark matter search results of the XENON1T experiment

P. DI GANGI([1])([2]) on behalf of the XENON COLLABORATION

([1]) *INFN, Sezione di Bologna - Bologna, Italy*
([2]) *Dipartimento di Fisica, Università di Bologna - Bologna, Italy*

received 15 February 2018

Summary. — The XENON1T experiment is the first ton-scale dual-phase (liquid-gas) xenon time projection chamber, currently in operation at the Laboratori Nazionali del Gran Sasso in Italy. The experiment aims at the dark matter direct detection exploiting a $\sim$ 2000 kg mass of liquid xenon as a target for interactions of weakly interacting massive particles (WIMPs) with xenon nuclei. We report the blinded search results of the first science run, using 34.2 live-days of data acquired between November 2016 and January 2017. The WIMP dark matter search is performed inside a (1042 ± 12) kg fiducial mass and in the [5,40] $\mathrm{keV_{nr}}$ energy range of interest, in which the electronic recoil background was $(1.93 \pm 0.25) \times 10^{-4}$ events/(kg×day×$\mathrm{keV_{ee}}$). Such a background level is the lowest ever achieved in a dark matter detector. The data analysis is performed with the profile likelihood approach and the observations result to be consistent with the background-only hypothesis, thus leading to exclusion limits on the spin-independent WIMP-nucleon interaction cross section for WIMP masses between 6 and 10^4 GeV/c^2. The most stringent limit is obtained for 35 GeV/c^2 WIMPs at 7.7×10^{-47} cm^2 with 90% confidence level (XENON COLLABORATION (Aprile E. *et al.*), *Phys. Res. Lett.*, **119** (2017) 181301), which is the lowest cross section ever probed to date.

1. – Introduction

A large number of indirect astronomical and cosmological observations provide a strong indication that dark matter exists [1, 2], meaning that new physics beyond the Standard Model (BSM) of particle physics is needed. Observational data, from the galactic to the cosmological scale, are precisely described by the Λ cold dark matter model [3, 4], which requires a non-relativistic non-baryonic component of the Universe, called *dark matter*, with an energy density of $\Omega_c h^2 = 0.1197 \pm 0.0022$ as measured by PLANCK [1]. Several BSM theories (*e.g.*, supersymmetry [5]) associate this energy density to a class of postulated dark matter particles known as weakly interacting massive particles (WIMPs) [6]. Earth-based ultra-low background detectors aim at directly

Creative Commons Attribution 4.0 License (http://creativecommons.org/licenses/by/4.0)

observing WIMPs as they are expected to scatter off the detectors' target nuclei, following a falling exponential nuclear recoil spectrum in the energy range of few keV [7].

The XENON1T experiment is the present step of the XENON dark matter project which aims at the direct detection of WIMPs through nuclear recoils (NR) from WIMP-nucleon scattering by operating dual phase (liquid-gas) time projection chambers (TPC) filled with a liquid xenon (LXe) target. The project started in 2008 with the prototype XENON10 [8, 9], featuring 25 kg of LXe and 14 kg target mass. The scalability of such detector allowed to move towards the XENON100 experiment [10] (161 kg total mass of LXe, 62 kg target mass), which published competitive results on spin-independent WIMP-nucleon interactions [11] in 2012, probing also other models of WIMP-nucleon interactions, axions and axion-like particles, and leptophilic dark matter interacting with atomic electrons. XENON1T is the first ton-scale dark matter experiment of this kind ever built and operated, with its $\sim$ 2000 kg of LXe target mass. It is located in the underground Laboratori Nazionali del Gran Sasso, in Italy, under about 1400 m of rock (3600 m water equivalent) ensuring the shielding from the cosmic radiation required for the experiments looking for such rare events as dark matter interactions are expected to be.

The goal of this experiment is to improve upon the XENON100 sensitivity by two orders of magnitude, probing yet unexplored spin-independent WIMP-nucleon scattering cross sections down to $1.6 \times 10^{-47}\,\mathrm{cm}^2$ for WIMP mass of $50\,\mathrm{GeV}/c^2$ in the full exposure of 2.0 t×y [12], while the projected sensitivity at low WIMP masses approaches the so-called "neutrino floor" [13], due to the irreducible background from coherent scattering of solar neutrinos off target nuclei.

The further step forward of the XENON project, XENONnT, is already planned and under preparation. It will rapidly replace XENON1T as most of the subsystems were designed to support a significantly larger dark matter detector with $\sim$ 6 tonnes LXe target. The physics reach of XENONnT is to improve the sensitivity to the spin-independent WIMP-nucleon interaction by another order of magnitude with respect to XENON1T [12].

2. – The XENON1T experiment

The XENON1T experiment uses a total mass of $\sim$ 3.2 tonnes of ultrapure liquid xenon contained in a double-walled vacuum cryostat in which a cylindrical dual phase TPC, 97 cm long and 96 cm wide, is installed. The mass of LXe enclosed within the TPC amounts to (2004 ± 5) kg, while the remaining $\sim$ 1200 kg of LXe acts as a passive shielding to the inner fiducial volume where the actual search for signal events is performed. Two arrays of 3 inches Hamamatsu R11410-21 photomultiplier tubes (PMTs) are arranged in the upper and lower ends of the TPC, counting 127 and 121 photosensors respectively, for a total of 248 PMTs. The TPC is enclosed by 24 interlocking PTFE (polytetrafluoroethylene) panels, properly treated to optimize their reflectivity for the scintillation light emitted by the LXe as a response to a scattering.

Particles entering the LXe target can, in fact, interact with atomic electrons (if γ rays and β electrons) or scatter off xenon nuclei (if neutrons or WIMPs), producing electron recoils (ER) or nuclear recoils (NR), respectively. The recoils excite and ionize the LXe and the proportion of energy lost between these two processes depends on the recoil type. This is therefore a feature that allows to discriminate a WIMP signal (NR) from electronic recoil backgrounds since the excitation and ionization signals can be measured independently with a dual phase TPC [14]. The prompt scintillation signal (called $S1$)

consists in the 178 nm scintillation light emitted by the de-excitation of Xe_2^* excimers eventually formed due to a recoil. The $S1$ signal is observed in both the PMT arrays. The energy lost into ionization is independently measured by means of a delayed secondary scintillation signal ($S2$) proportional to the amount of ionization electrons [15]. These charges, generated in the recoil, are drifted away from the interaction vertex towards the liquid-gas interface thanks to a (116.7 ± 7.5) V/cm electric field across the TPC established between two grid electrodes: the cathode, negatively biased, placed at the bottom of the TPC, and the gate, at ground potential, on the top, few millimetres below the liquid-gas interface. The survival probability of the electrons depends on the drift length through an exponential function whose time constant, called *electron lifetime*, is related to the level of electronegative impurities present in LXe. A second >10 kV/cm electric field is applied employing a positively biased electrode (anode) to extract the electrons from the liquid phase and to provide them with sufficient energy to generate a proportional scintillation signal in the ∼7 cm gap of gaseous xenon (GXe) below the top PMT array.

The time delay between the $S1$ and the $S2$ signals provides the information on the z coordinate of the primary interaction site, while the position in the orthogonal (x,y) plane is determined by the pattern of top PMTs that detect the localized $S2$ signal. The position of interactions can therefore be fully reconstructed in 3 dimensions and from the position and the number of $S2$ signals observed also the scatter multiplicity can be determined, allowing to distinguish single scatters (expected for WIMP interactions) from multiple scatters of background events. The $S2/S1$ ratio is a valuable parameter to reject electronic recoil background as this is larger for ER events and typically a $> 99.5\%$ ER discrimination is achieved mantaining a 50% signal (NR) acceptance.

The cryostat containing the TPC is placed in the centre of a cylindrical tank of 9.6 m of diameter and 10.2 m of height. The tank is filled with deionized water and instrumented with 84 PMTs to form an active water Cherenkov detector [16], besides providing effective shielding against γ rays and neutrons from natural radioactivity in the experimental hall. This ancillary detector is operated as a Cherenkov Muon Veto (MV) since it identifies muons and muon-induced neutrons, allowing to veto events detected in the TPC in coincidence with MV signals.

All the auxiliary systems, such as the cryogenics plant, the xenon storage and recovery, the cryogenic distillation pump for krypton removal, the xenon gas and purification systems, the data acquisition (DAQ) and slow control systems, are hosted in a three-floor service building adjacent to the water tank.

3. – The first XENON1T science run

The dark matter search data taking of XENON1T started on 22 November 2016, after few months of commissioning phase. The science run ended on 18 January 2017 when an earthquake in the area of the LNGS temporarily interrupted detector operations, providing a natural break for the first short-lasting run. In such period the experiment collected 34.2 live-days of blinded data for dark matter search.

The detector has been operated in stable conditions at (177.08 ± 0.04) K temperature and (1.934 ± 0.001) bar pressure. During the science run the electron lifetime increased from 350 to 500 μs (with 452 μs average value) thanks to continuous circulation of xenon in gas phase through hot metal getters which purify the xenon gas by trapping electronegative impurities. The maximum drift time, for interactions occurring in the bottom of the TPC, is 673 μs.

The concentration of intrinsic contaminants which contribute to the low energy background was reduced during data taking. In particular, $^{\mathrm{nat}}$Kr was removed from LXe using a column for cryogenic distillation [17], lowering its initial concentration by a factor $\sim$7 at the end of the science run. Also the ^{222}Rn concentration was reduced by $\sim$20% using the krypton distillation column in inverse mode [18]. The resulting ER background rate, dominated by ^{214}Pb β decay (part of the ^{222}Rn decay chain) in the low energy range of interest for WIMP searches, was estimated in $(0.8\text{–}1.9) \times 10^{-4}$ events/(kg$\times$day$\times$keV$_{\mathrm{ee}}$), which is the lowest ER background ever achieved in a dark matter detector.

The PMT high voltage was kept stable, while 27 PMTs were turned off and 8 were excluded from the analysis due to low single-photoelectron detection efficiency. The PMT gains and afterpulse rates were monitored twice a week with dedicated calibration LED data [19].

In order to calibrate the detector response to physical interactions, calibration runs took place right before or during the science run. Specifically, calibration data taking consisted in 3.3 days of $^{83\mathrm{m}}$Kr data, for the spatial dependence of detector's response, 3.0 days of ^{220}Rn, for low energy ERs, and 16.3 days of ^{241}AmBe, for low energy NRs.

The DAQ system continuously recorded signals from individual PMT channels with average live time of 92% during the science run. The trigger efficiency for $S2$ signals larger than 200 photoelectrons (PE) was 99%.

3˙1. *Data analysis and detector characterization.* – Raw data are processed using the PAX (Processor for analyzing XENON) software to elaborate photon hits in each PMT, cluster them and classify group of hits as $S1$ or $S2$ signals. For $S1$s, a three-fold coincidence within 50 ns is required. Monte Carlo simulations of raw waveforms are exploited to tune the reconstruction algorithms and to assess the detection efficiency for signal (NR) events. The Monte Carlo code used reproduces the interaction physics, the light propagation in the TPC and the electronics chain, and it was validated against $^{83\mathrm{m}}$Kr and ^{220}Rn data.

The observables in the analysis are corrected for detector effects. The interaction position is corrected for drift field non-uniformities from a finite element simulation validated against $^{83\mathrm{m}}$Kr calibration data. The $S2$ signal size is corrected for the electron loss in the drift through the measured electron lifetime. The light collection efficiency (LCE) of both $S1$ and $S2$ signals is mapped using $^{83\mathrm{m}}$Kr data to correct for photon loss during the propagation in the TPC. The resulting variables with such corrections are called $cS1$ and $cS2$. This analysis uses the $S2$ signals only detected in the bottom PMTs ($cS2_{\mathrm{b}}$) as the response to $S2$ light is more homogeneous than in the top PMT array.

The energy scale of physical events is determined by fitting the anti-correlation between the $cS1$ and $cS2_{\mathrm{b}}$ for signals of known energy, from 40 keV to 1 MeV, and linearity across this energy range is found. The derived photon gain g_1 corresponds to (0.144 ± 0.007) PE/photon, while the electron gain is $g_2 = (11.5 \pm 0.8)$ PE/electron. The combined energy scale, which exploits the information from both $S1$ and $S2$, is then obtained by $E = (n_{ph} + n_e) \cdot W = (\frac{cS1}{g_1} + \frac{cS2_b}{g_2}) \cdot W$, where $W = 13.7$ eV is the average energy required to create a quantum (photon or electron) in LXe. The light and charge yields time evolution is monitored with $^{83\mathrm{m}}$Kr calibrations and results are stable within 0.77% and 1.2%, respectively.

The models describing the response to ERs and NRs in the low energy range of interest for WIMP searches are fitted to ^{220}Rn and ^{241}AmBe calibration data (shown in fig. 1). The ER model is based on a simulation of the detector response and describes the conversion of energy depositions from electronic recoils into the observable signals $cS1$

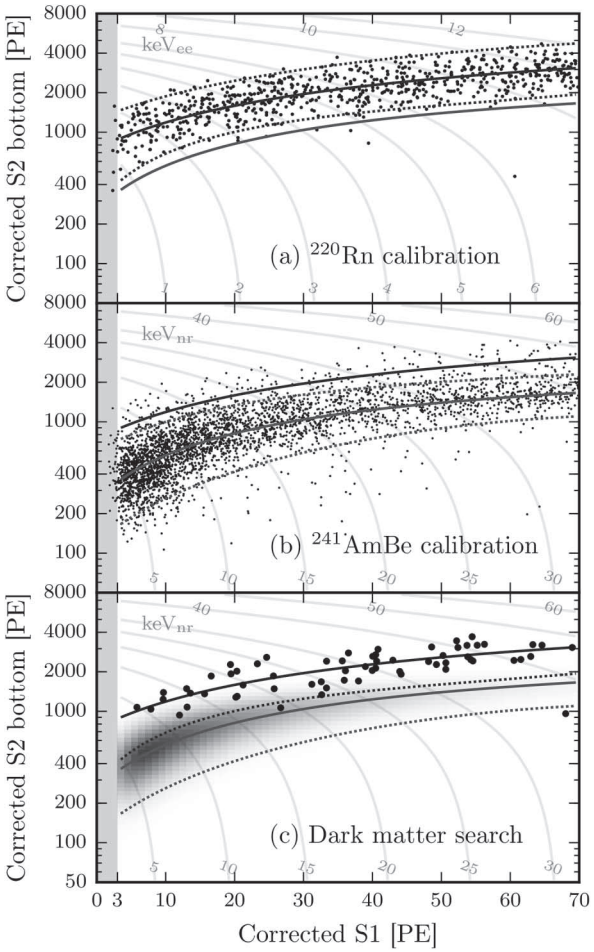

Fig. 1. – Observed data in $cS2_b$ *vs.* $cS1$ for (a) ^{220}Rn ER calibration, (b) ^{241}AmBe NR calibration, and (c) the 34.2 day dark matter search. Solid and dotted lines indicate the median and $\pm 2\sigma$ quantiles, respectively, of simulated event distributions (with the simulation fitted to calibration data). The lower solid line shows NR (fitted to ^{241}AmBe) and the upper line ER (fitted to ^{220}Rn). In (c), the shaded distribution indicates the signal model of a 50 GeV/c^2 WIMP. Thin gray lines and labels indicate contours of the constant combined energy scale in keV for (a) ER and (b), (c) NR. Data below $cS1 = 3$ PE (the gray region) are not in our analysis region of interest and are shown only for completeness.

and $cS2_b$. The best-fit (on ^{220}Rn data) of the main parameters of the model, *i.e.*, photon yield and recombination fluctuations, are comparable with those in [20]. The model for the response to NRs shares the same detector parameters but relies on a different model and parametrization of the conversion of energy into scintillation signals from the NEST model [21]. The XENON1T response to NRs is obtained by fitting this model to ^{241}AmBe data.

The expected signals from WIMPs are low-energy single-scatter NRs. Therefore, several event selection cuts are applied to data: 1) a single $S2$ larger than 200 PE must be present and any other $S2$ must be compatible with single electrons from photoionization or delayed extraction; 2) an event must not closely follow high energy events; 3) the

TABLE I. – *Expected number of events for each background component in the fiducial mass; in the full cS1∈[3,70] PE, $cS2_b \in [50, 8000]$ PE search region and in a reference region between the NR median and the -2σ quantile in $cS2_b$. Uncertainties < 0.005 events are omitted. The ER rate is unconstrained in the likelihood; for illustration, we list the best-fit values to the data in parentheses.*

	Full ROI	Reference
Electronic recoils (ERs)	(62 ± 8)	$(0.26^{+0.11}_{-0.07})$
Radiogenic neutrons (n)	0.05 ± 0.01	0.02
CNNS (ν)	0.02	0.01
Accidental coincidences (acc)	0.22 ± 0.01	0.06
Wall leakage (wall)	0.5 ± 0.3	0.01
Anomalous (anom)	$0.10^{+0.10}_{-0.07}$	0.01 ± 0.01
Total background	63 ± 8	$0.36^{+0.11}_{-0.07}$
$50\,\mathrm{GeV}/c^2$ WIMP ($\sigma = 10^{-46}\,\mathrm{cm}^2$)	1.66 ± 0.01	0.82 ± 0.06

time spread of $S2$ signals must be consistent with the drift length; 4) the $S1$ and $S2$ hit patterns must be consistent with the reconstructed position; 5) the uncorrelated single electrons and PMT dark counts before the $S2$ must be less than 300 PE. The acceptance of all the selection cuts applied on single-scatter NR events is 82% in the energy range $[5{,}40]\,\mathrm{keV_{nr}}$. The efficiency of cuts is evaluated using simulated events or control samples from calibration data.

For this analysis we select a cylindrical fiducial volume which includes $(1042 \pm 12)\,\mathrm{kg}$ of LXe mass, based on the reconstructed spatial distribution of ER background events in the dark matter search data. The region of interest (ROI) in the observable space is defined as $cS1\in[3{,}70]$ PE and $cS2_\mathrm{b}\in[50{,}8000]$ PE.

Several components contribute to the background for the WIMP search. The background expectations are intended inside the fiducial mass and in the ROI. However, we also list the expected rate in a reference sub-region of the ROI which would contain about the 50% of candidate signal events, while excluding 99.6% of the ER background, even if the statistical inference is done with a profile likelihood analysis in the entire ROI. The reference region is between the NR median and its -2σ quantile boundary. Table I reports the expectation values of the background components, while the $cS1$ spectrum of the background models in the reference region is plotted in fig. 2.

The ER background (ERs) component in the ROI is primarly due to β decays of ^{85}Kr and ^{214}Pb and has an almost flat energy spectrum, while the ER background from radioactive decays in the detector materials is suppressed by the choice of the fiducial volume. We have measurements of ^{85}Kr and ^{214}Pb concentrations, but the most stringent constraint on ERs is obtained from the dark matter search data. Therefore, the ER background is not a fixed parameter in the likelihood analysis.

The NR background includes radiogenic neutrons (n) produced by (α, n) or spontaneous fission in the detector materials, coherent scattering of neutrinos off xenon nuclei (CNNS) and muon-induced neutrons which are estimated to contribute $\mathrm{O}(10^{-3})$ events thanks to the presence of the Muon Veto. This last component is then negligible and not included in the background model.

Accidental coincidences (acc) of uncorrelated $S1$s and $S2$s are estimated from the observed rate of isolated $S1$ and $S2$ signals: $(0.78 \pm 0.01)\,\mathrm{Hz}$ and $(3.23 \pm 0.03)\,\mathrm{mHz}$, respectively. Isolated $S1$s are generated from events where the charge is completely lost

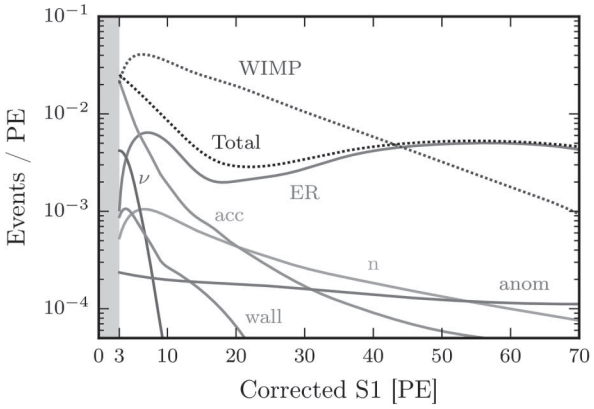

Fig. 2. – Background model in the fiducial mass and in a reference region between the NR median and the -2σ quantile in $cS2_b$, projected onto $cS1$. Solid lines show the expected number of events from individual components listed in table I; the labels match the abbreviations shown in the table. The dotted black line "Total" shows the total background model, while the dotted line "WIMP" shows a $50\,\mathrm{GeV}/c^2$ WIMP signal, with $\sigma = 10^{-46}\,\mathrm{cm}^2$, for comparison.

due to poor collection efficiency, as it is the case for recoils happened below the cathode. Photoionization at the electrodes or delayed extraction can originate isolated $S2$s. The energy spectrum of this population is expected at lower $cS2_b$ than typical NRs.

The wall leakage (wall) background is due to inward-reconstructed events happened close to the TPC's lateral wall. Part of the charge is lost at the wall causing unusually low $cS2_b$ letting ER events to leak in the region of the ROI where NRs are expected.

Finally, we include a small background with uniform spectrum in the ($cS1$, $\log cS2_b$) space with an anomalous low $cS2_b$. Such component was already observed in XENON100 [22] and a candidate event for such population is observed in the ^{220}Rn calibration data. The origin of these events is under investigation.

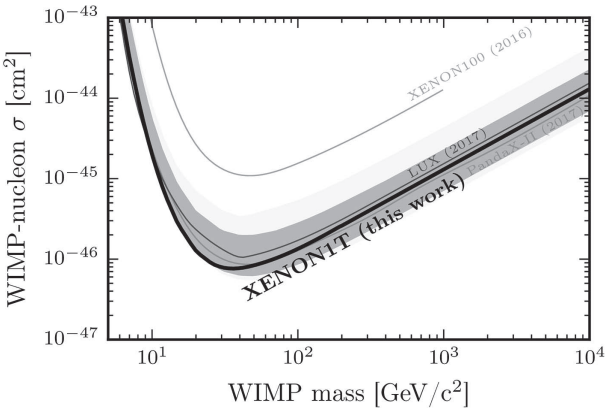

Fig. 3. – The spin-independent WIMP-nucleon cross section limits as a function of the WIMP mass at 90% confidence level for this run of XENON1T. The shaded intervals are the 1σ and 2σ sensitivity bands. Results from LUX [23], PandaX-II [24], and XENON100 [22] are shown for reference.

3˙2. *Data unblinding and statistical interpretation.* – We followed a blinded data analysis procedure, meaning that a predefined signal box was blinded until the event selection criteria, the fiducial mass and the background models were definitively fixed. The data unblinding revealed 63 events in the ROI passing the selection cuts and inside the fiducial volume (fig. 1(c)), in the science run exposure of 0.098 t×y. None of these events are in coincidence with a Muon Veto signal. Two events are below the -2σ ER quantile. The event at $cS1$=26.7 PE is 2.4σ below the ER median. The other event at $cS1$=68.0 PE is even below the -2σ NR quantile, showing no compatibility neither with any of the background models nor with the signal model. This event was carefully scrutinized, but no good reasons to discard it were found.

The ER rate observed is $(1.93 \pm 0.25) \times 10^{-4}$ events/(kg × day × $\mathrm{keV_{ee}}$), compatible with our prediction in [12] of $(2.3 \pm 0.2) \times 10^{-4}$ events/(kg × day × $\mathrm{keV_{ee}}$), after accounting for the actual $^{\mathrm{nat}}$Kr concentration measured during the science run.

To probe the WIMP signal hypothesis we make use of an extended unbinned profile likelihood test statistic in the observable space ($cS1$, $cS2_{\mathrm{b}}$). The uncertainties on the background rates, shown in table I, are propagated to the likelihood function as nuisance parameters as well as the uncertainties on the most significant shape parameters of the ER and NR models inferred from the posteriors of the calibration fits. The procedure in [25] was also followed to account for mismodeling of the ER background.

The signal model tested assumes a standard isothermal WIMP galactic halo of density $\rho_{DM} = 0.3\,\mathrm{GeV/cm^3}$ with standard values of parameters and nuclear cross section as described in [26]. Light and charge yields for WIMPs are conservatively assumed to be zero for recoils below 1 keV.

The data are consistent with the background-only hypothesis, which is the best fit for any WIMP mass. The exclusion limit setting procedure was therefore followed to assess the spin-independent WIMP-nucleon cross section value excluded at 90% confidence level for WIMP masses in the range 6–10000 GeV/c^2. The power constraint approach is used to avoid large underfluctuations of the exclusion limit, imposing a lower bound at -1σ level of the sensitivity band [27]. The limit obtained improves upon the XENON100 results by one order of magnitude as shown in fig. 3. The minimum at $7.7 \times 10^{-47}\,\mathrm{cm^2}$ for $35\,\mathrm{GeV}/c^2$ WIMPs is currently the strongest exclusion limit.

The sensitivity of XENON1T continued to improve since the experiment kept recording data for dark matter search after resuming normal operation shortly after the earthquake of January 2017. The new results with much larger exposure will be released in the next future.

REFERENCES

[1] PLANCK Collaboration (Ade P. A. R *et al.*), *Astron. Astrophys.*, **594** (2016) A13.
[2] Springel V. *et al.*, *Nature*, **435** (2005) 629.
[3] Dodelson S., *Modern Cosmology* (Academic Press, Amsterdam) 2003.
[4] Kolb E. W. and Turner M. S., *Front. Phys.*, **69** (1990) 1.
[5] Jungman G., Kamionkowski M. and Griest K., *Phys. Rep.*, **267** (1996) 195.
[6] Steigman G. and Turner M. S., *Nucl. Phys. B*, **253** (1985) 375.
[7] Goodman M. W. and Witten E., *Phys. Rev. D*, **31** (1985) 3059.
[8] XENON10 Collaboration (Angle J. *et al.*), *Phys. Rev. Lett.*, **100** (2008) 021303.
[9] XENON10 Collaboration (Aprile E. *et al.*), *Astropart. Phys.*, **34** (2011) 679.
[10] XENON100 Collaboration (Aprile E. *et al.*), *Astropart. Phys.*, **35** (2012) 573.
[11] XENON100 Collaboration (Aprile E. *et al.*), *Phys. Rev. Lett.*, **109** (2012) 181301.

[12] XENON Collaboration (Aprile E. *et al.*), *JCAP*, **04** (2016) 027.
[13] Billard J., Strigari L. and Figueroa-Feliciano E., *Phys. Rev. D*, **89** (2014) 023524.
[14] Aprile E. *et al.*, *Phys. Rev. Lett.*, **97** (2006) 081302.
[15] Lansiart A. *et al.*, *Nucl. Instrum. Methods*, **135** (1976) 47.
[16] XENON1T Collaboration (Aprile E. *et al.*), *JINST*, **9** (2014) 072008.
[17] XENON Collaboration (Aprile E. *et al.*), *Eur. Phys. J. C*, **77** (2017) 275.
[18] Lindemann S. and Simgen H., *Eur. Phys. J. C*, **74** (2014) 2746.
[19] Saldanha R., Grandi L., Guardincerri Y. and Wester T., *Nucl. Instrum. Methods Phys. Res. Sect. A*, **863** (2017) 35.
[20] LUX Collaboration (Akerib D. S. *et al.*), *Phys. Rev. D*, **93** (2016) 072009.
[21] Lenardo B. *et al.*, *IEEE Trans. Nucl. Sci.*, **62** (2015) 3387.
[22] Aprile E. *et al.*, *JCAP*, **05** (2017) 013.
[23] LUX Collaboration (Akerib D. S. *et al.*), *Phys. Rev. Lett.*, **118** (2017) 021303.
[24] PandaX-II Collaboration (Cui X. *et al.*), *Phys. Rev. Lett.*, **119** (2017) 181302.
[25] XENON Collaboration (Aprile E. *et al.*), *Phys. Rev. D*, **94** (2016) 122001.
[26] Lewin J. and Smith P., *Astropart. Phys.*, **6** (1996) 87.
[27] Cowan G. *et al.*, preprint arXiv:1105.3166.